SPACE TELESCOPE SCIENCE INSTITUTE
Operated for NASA by AURA

Instrument Science Report TEL 2005-01

Observer Anomaly(?): Recent Jitter and PSF Variations

R. L. Gilliland

gillil@stsci.edu

February 2005

Abstract

An anomaly in the HST Pointing Control System (PCS) has been noticed since June 2004 which results in an increased level of gyro bias in V3, generally at the time HST enters orbital day. This ISR documents Point Spread Function (PSF) and pointing drifts from a recent 5-orbit program with the HRC of ACS. These Grism observations of a bright star were taken in a time-series mode of 95 second integrations, without dithering, for five consecutive orbits on a bright target allowing for unusually high precision measurement of changes in PSF or pointing. Near the time orbital night starts there is a spike in the V3 rms guiding as reported in associated jitter files, at the same time the PSF as measured from the spectrum width shows a transition to larger widths. The correlation between jitter as reported by the PCS, and that measured from the data is only moderately good. The jitter as derived from the data stays high for extended periods while the jitter files report transition back to standard levels.

1. Introduction

The DD/GO-10441 program is intended to provide high S/N time-series photometry of the recently discovered transiting planet system TrES-1 (Alonso et al. 2004). Observations

in 2000 using STIS to disperse the light from HD 209458 (V = 7.54) over a large number of pixels allowed time series photometry with a S/N of over 9,000 per 60 second observation. At V = 11.79 the higher efficiency of the ACS/HRC grism compared to what had been available with STIS, provides a S/N of nearly 7,000 per 95 second integration. I report on an anomalous variation of the PSF widths associated with these observations, which may be correlated with the PCS Observer Anomaly.

2. Data Analyzed in this Study

The observations of TrES-1 were planned in order to return optimal high signal-to-noise photometry with the assumption that the full G800L spectra from each exposure would simply be summed over. Peak per pixel count levels of 109,000 electrons are reached with these GAIN = 2 exposures providing a per pixel S/N of 330. Summing over the approximately 10,000 pixels enclosing 99% of the flux in the first order G800L spectrum results in 4.5×10^7 electrons for a Poisson-limited S/N of 6,700. Simple aperture extractions of counts have provided a resulting S/N of 6,100 per time point as measured by the rms of 42 points in the two HST orbits taken outside of the TrES-1 transit.

Positions and characteristic scales of PSFs can typically be measured to a precision of order the inverse S/N multiplied by the PSF width. In this case the PSF width (FWHM) is about 3.5 pixels (after broadening by a near 45 degree projection in x, y coordinates), which should support position or width measurements on a per exposure basis to order 3.5 pixels × 25 mas/pixel divided by the S/N, or approximately 0.01 mas. Assuming that the PSF is Gaussian, convolution with jitter also assumed to have a Gaussian function shape, results in PSF scales of the intrinsic PSF scale and jitter blurring adding in quadrature. This in turn implies that a 0.01 mas sensitivity should support detection of jitter changes at the level of about 0.03 mas of jitter rms.

Table 1 lists the HRC G800L observations all of which are from DOY 324 in 2004. The Start time is taken from the header keyword TIME-OBS (UT time of start of observation). The Time (HJD) is the Heliocentric Julian Date at time of mid-exposure (with 53000 subtracted). V2-rms and V3-rms are the time-averaged jitter in units of milli-arcsec taken from keywords V2_rms and V3_rms in the _jif.fits files for the corresponding observations. The final two columns give the average width (see discussion in the next section) of the spectrum projected along rows and columns respectively in units of milli-arcsec for the full-width-half-maximum.

To keep readout overheads low these observations were taken using the 513×512 subarray HRC-512. One image is shown in Figure 1. Zeroth order of the G800L spectrum is near the upper left, the first order spectrum starts (at about 5500 Å) near the center and terminates (at about 10700 Å) at the local minimum near the lower right. Only part of the second order G800L spectrum falls within the field of view. The HRC is oriented in the HST focal plane such that the detector y-axis is almost identically parallel (to within 0.1 degree) to V3, while the x-axis is about 5 degrees (non-orthogonal due to geometric distortion) from -V2.

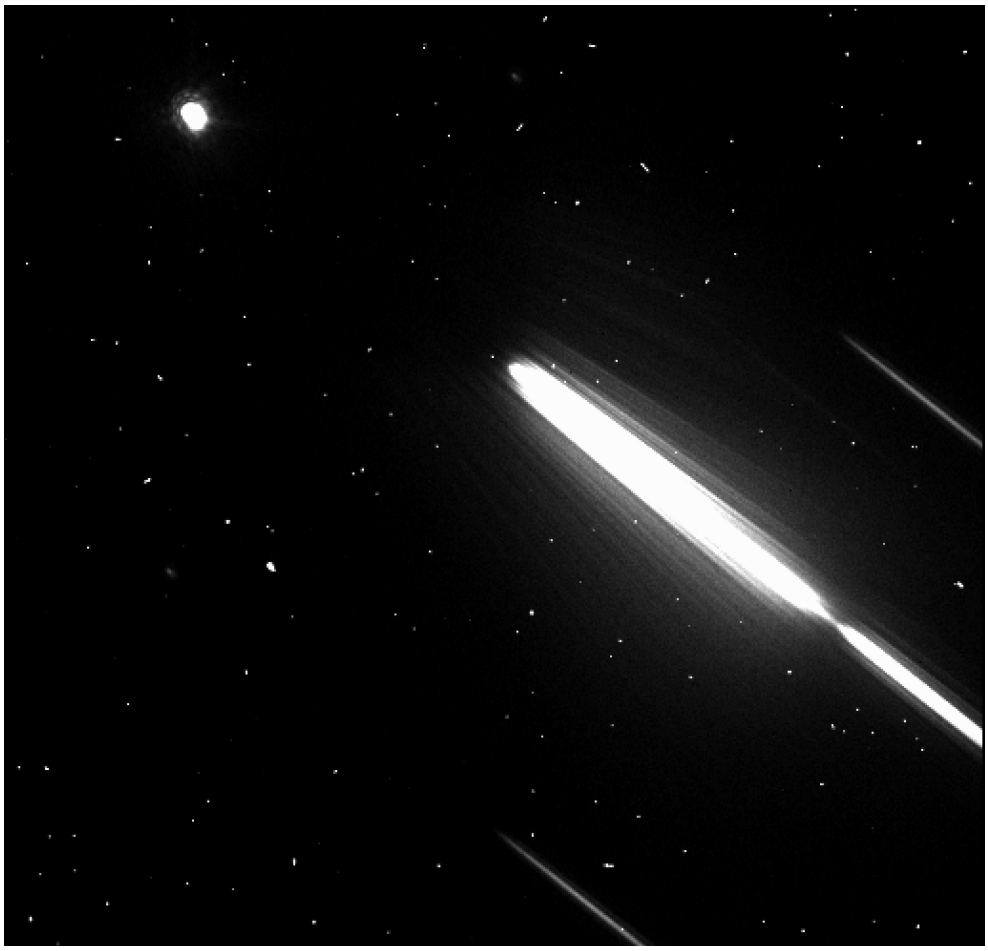

Fig. 1.— Image of G800L spectrum for TrES-1 from GO/DD-10441.

3. Analyses

All of the analyses reported here start with the individual _flt.fits files that included overscan bias and dark subtraction. Grism data from the pipeline are not flat-fielded, since the flat-field to be used needs to account for wavelength dependence along the spectra of interest. Using information on the HRC grism from ACS ISR 03-07 (Pasquali, Pirzkal, and Walsh 2003) I have defined an effective wavelength as a function of distance along the first order spectrum, and assumed this is constant along columns. Then a flat-field is defined as a function of wavelength by fitting a quadratic to the pixel-to-pixel flat field values in the full set of broad-band filter flats spanning the G800L sensitivity. This provides a flat field containing the requisite wavelength dependence for this specific observation that is then divided into each of the _flt.fits data files before further analysis. The analysis and interpretation of HRC grism data is complicated by having the spectrum at a steep angle

of -38 degrees with respect to the CCD x-axis. I have performed analyses by fitting a one-dimensional Gaussian to data values in cuts in both columns and rows centered on the spectrum peak, yielding position, and width at each column or row.

The resulting Gaussian widths are significantly (roughly sqrt(2)) broadened simply by the near-45 degree projection relative to detector coordinates. The actual factors are 1.62 in x, and 1.27 in y, and the different widths for row and column fits are completely accounted for by this factor, plus the slightly differing plate scales.

The resulting drift in y is given by averaging over separate fits over the 125 columns in the spectrum with high signal and is shown in Figure 2.

The amount of position drift is a full range of about 0.3 pixels, or 8 mas each orbit, with an additional offset of about 2 mas orbit-to-orbit – values that are within normal bounds.

The derived Gaussian widths as a function of wavelength are nearly constant below 7000 Å, but become significantly broader at wavelengths beyond this. Such a dependence is expected from the small HRC pixels and the relative contribution of over-sampling of the diffraction limit as the latter grows to the red. I have therefore adopted a mean over 25 columns from 5630 – 6330 Åto derive a measure of the mean PSF width in each exposure. The resulting variations are shown in Figure 3.

Clearly there is an apparent correlation of excess jitter with the transition from orbital day to night, but this is the opposite phase generally associated with the Observer Anomaly. There is an excellent temporal correlation between the onset of excess jitter each orbit, and reported jitter values from the PCS. However, the jitter derived from the data stays high, while the PCS based jitter files always show values transitioning back to zero.

To avoid any ambiguities in interpreting increased PSF widths given the use of grism spectra that are at a steep angle to CCD x,y coordinates, I have generated a series of model spectra with differing levels of pure V3 rms jitter and measured the resulting change of width. The resulting variation of measured FWHM-y for assumed jitter of 0.0, 3.5, 8.0 and 12.0 mas in V3 (parallel to detector y) is shown in Figure 4.

In the simulated data the imposition of jitter only along V3 results in measured increases of jitter in both x, and y CCD coordinates by projection, and at relative amplitudes nearly identical to that from the actual data. These analyses are therefore not useful for isolating in which axis the actual jitter may exist. Under the assumption that the excess jitter seen in FWHM-y for Figure 3 results from V3 jitter only, then it is now possible to accurately estimate the required amplitude. Further complicating interpretation

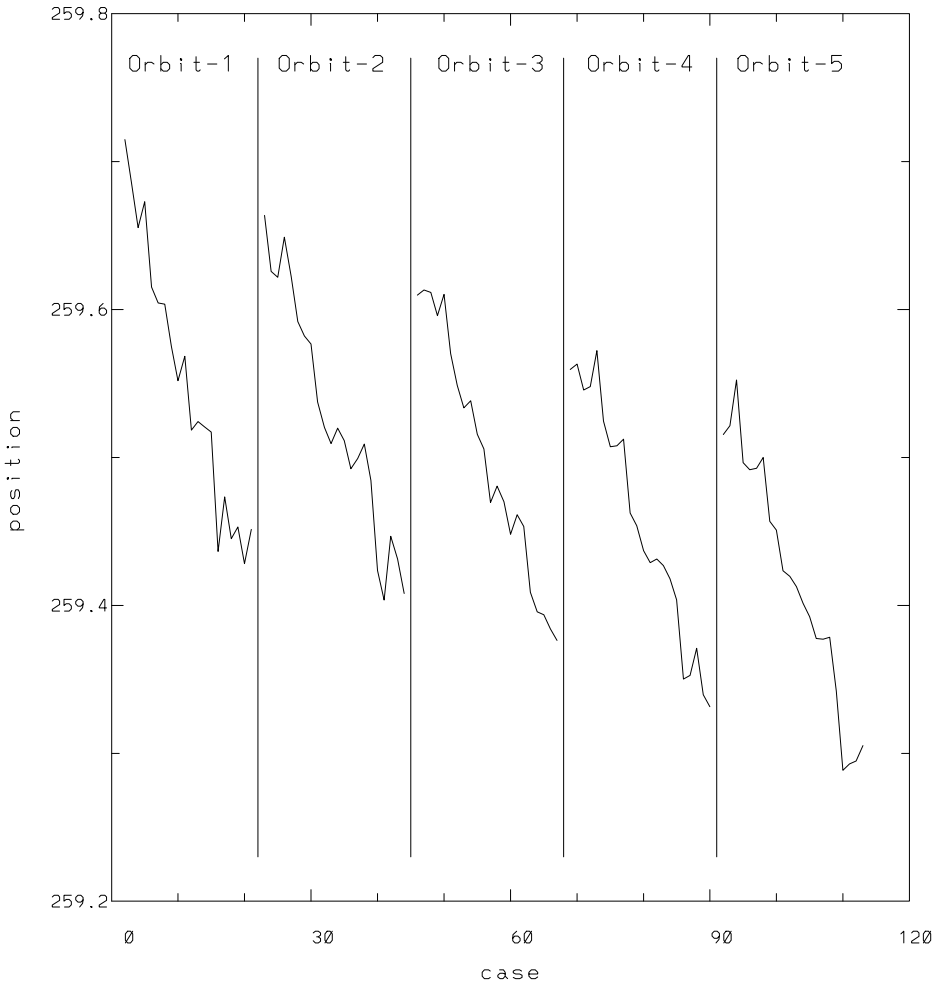

Fig. 2.— Position drift in units of HRC pixels along y for each of the 108 exposures shown grouped by HST orbit number.

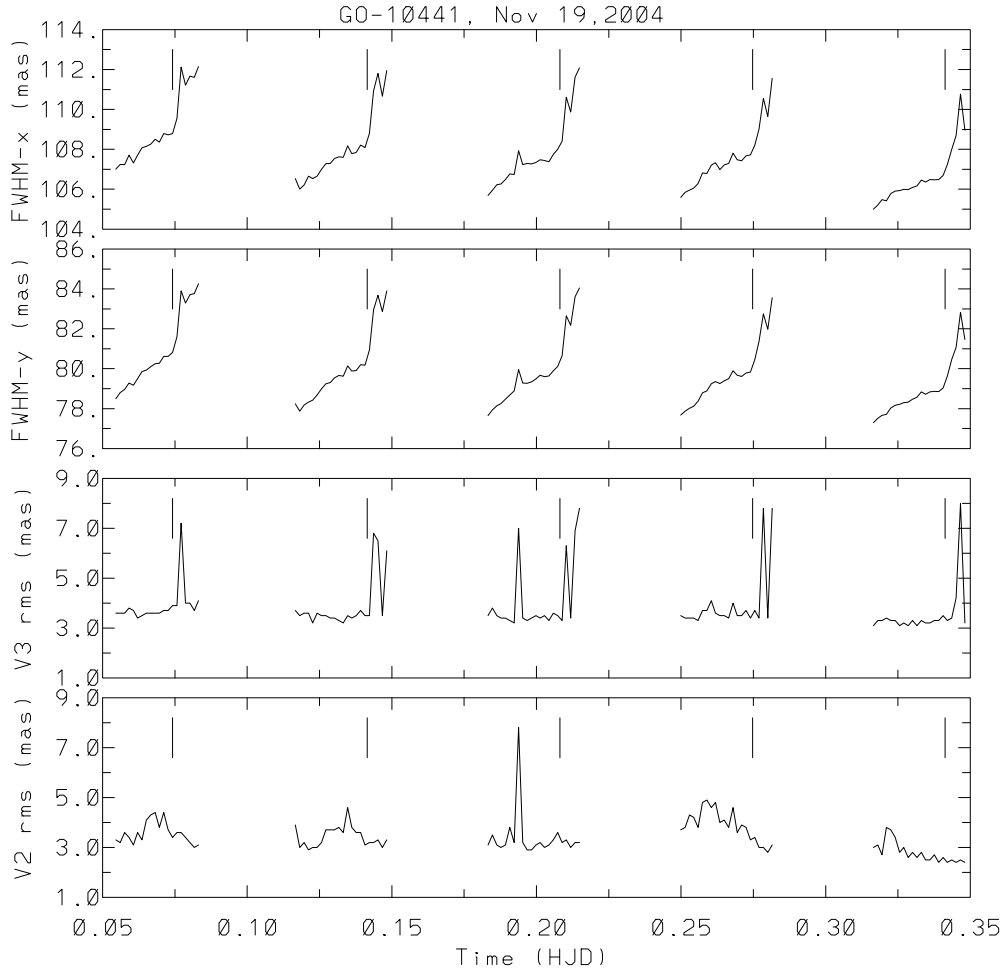

Fig. 3.— The upper two panels show full-width-half-maxima for Gaussian fits averaged over rows (x), and columns (y). Plotted against the same HJD times are the V2_rms and V3_rms values from the jitter files. Vertical tick marks indicate times that HST transitioned from orbital day to night.

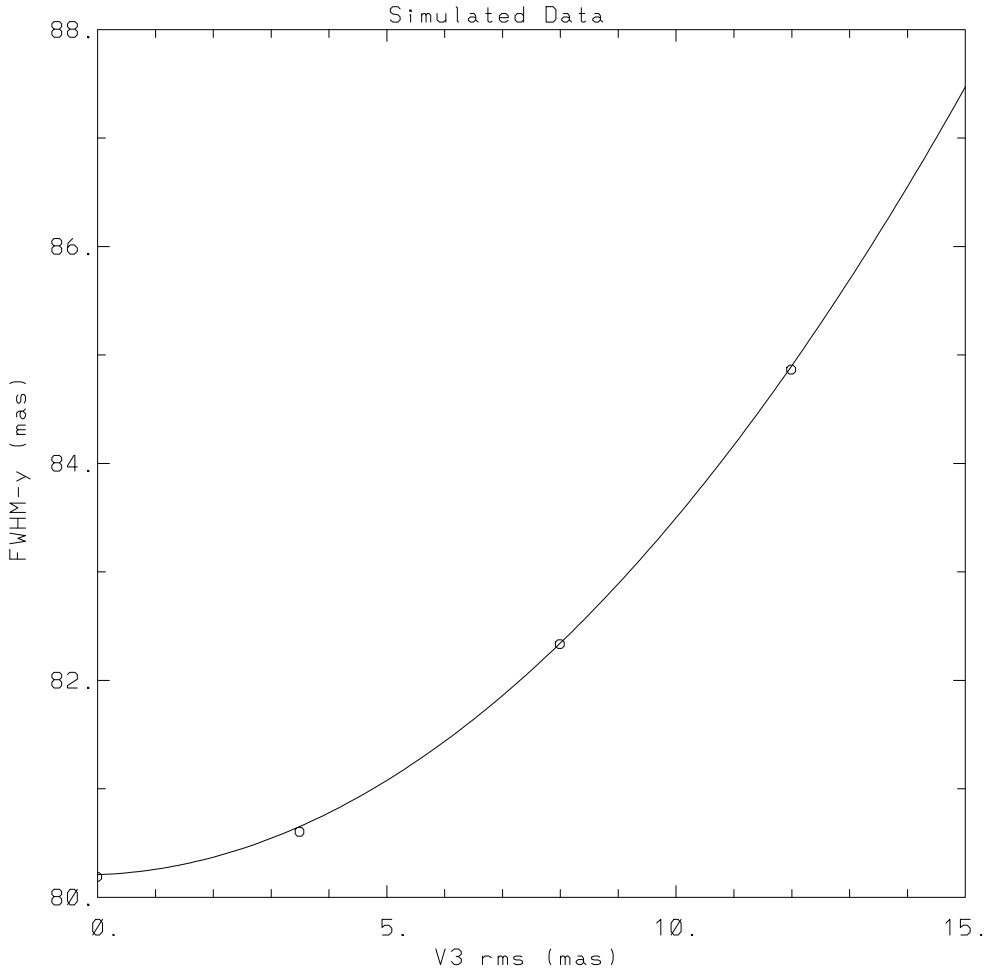

Fig. 4.— The variation of FWHM-y in mas for simulated data as a function of imposed rms jitter in the V3 axis. The curve is a quadratic fit to the variations.

is that the FWHM values are clearly trending upwards before the time of orbital day to night transition to higher values. I speculate that the slow drift may result from OTA breathing effects, and assume that this component remains continuous throughout the orbit. I have measured the mean amplitude of V3 rms jitter associated with the high state by averaging the FWHM-y at 18 points in the high state, and differencing this with the FWHM-y which would result from just extrapolating the near linear drift each orbit preceding the transition. This results in a mean delta of 2.21 mas in FWHM-y attributed to excess V3 jitter in the high state. Assuming an average V3 rms jitter of 3.5 mas before this, application of the quadratic function in Figure 4 implies an average jitter during the high states of 8.95 ± 0.05 mas. By contrast to a mean jitter of 8.95 mas for 18 observations as derived from the spectral data, the geometric mean of these points from the jitter files is only 5.87 mas with a maximum value of 8.0. The largest inferred jitter for one of these 95 s integrations is about 12 mas.

During the third orbit an isolated point during the first half of the orbit has reported jitter values of V2 = 7.8 mas, V3 = 7.0 mas. The jitter inferred from the data does show a local peak at this time, but the relative increase is very small compared to that seen at the end of each orbit. If V2 and V3 excursions were strongly correlated, producing excursions along the spectral dispersion, then it would be possible to have large V2 and V3 jitter not reflected in the PSF widths measured from these data. From inspection of the associated jitter ball, this does not seem a viable explanation. It would appear that the reported V2, V3 jitter integrals are only loosely correlated with reality.

Acknowledgements

I thank Stefano Casertano for discussions, and Colin Cox for providing data summaries from associated jitter files.

References

Alonso, R., Brown, T. M. *et al.* 2004, astro-ph/ 0408421.

Pasquali, A., Pirzkal, N., & Walsh, J. R. STECF ISR ACS 2003-07.

Table 1: Exposures obtained DOY 324 of 2004 as G800L time-series in GO/DD-10441.

Rootname	Start (UT)	Time (HJD)	V2-rms	V3-rms	FWHM-x	FWHM-y
j95q03sdq	13:19:18	329.05458	3.3	3.6	107.01	78.49
j95q03seq	13:21:28	329.05608	3.2	3.6	107.24	78.80
j95q03sfq	13:23:38	329.05759	3.6	3.6	107.23	78.97
j95q03sgq	13:25:48	329.05909	3.4	3.8	107.71	79.28
j95q03shq	13:27:58	329.06060	3.1	3.7	107.31	79.17
j95q03siq	13:30:08	329.06210	3.6	3.4	107.70	79.50
j95q03sjq	13:32:18	329.06361	3.3	3.5	108.08	79.86
j95q03skq	13:34:28	329.06511	4.1	3.6	108.15	79.93
j95q03slq	13:36:38	329.06662	4.3	3.6	108.26	80.10
j95q03smq	13:38:48	329.06812	4.4	3.6	108.51	80.26
j95q03snq	13:40:58	329.06963	3.8	3.6	108.36	80.28
j95q03soq	13:43:08	329.07113	4.4	3.7	108.79	80.61
j95q03sqq	13:45:18	329.07263	3.7	3.7	108.73	80.61
j95q03srq	13:47:28	329.07414	3.4	3.9	108.78	80.82
j95q03ssq	13:49:38	329.07564	3.6	3.9	109.55	81.59
j95q03stq	13:51:48	329.07715	3.6	7.2	112.12	83.91
j95q03suq	13:53:58	329.07865	3.4	4.0	111.21	83.29
j95q03svq	13:56:08	329.08016	3.2	4.0	111.67	83.71
j95q03swq	13:58:18	329.08166	3.0	3.7	111.61	83.77
j95q03sxq	14:00:28	329.08317	3.1	4.1	112.15	84.26
j95q03szq	14:48:39	329.11663	3.9	3.7	106.54	78.24
j95q03t0q	14:50:49	329.11813	3.0	3.5	106.00	77.87
j95q03t1q	14:52:59	329.11964	3.2	3.6	106.21	78.17
j95q03t2q	14:55:09	329.12114	2.9	3.6	106.65	78.33
j95q03t4q	14:57:19	329.12265	3.0	3.2	106.54	78.42
j95q03t5q	14:59:29	329.12415	3.0	3.6	106.65	78.69
j95q03t6q	15:01:39	329.12566	3.2	3.5	106.99	78.98
j95q03t7q	15:03:49	329.12716	3.7	3.5	107.28	79.24
j95q03t8q	15:05:59	329.12866	3.7	3.4	107.29	79.30
j95q03t9q	15:08:09	329.13017	3.7	3.4	107.54	79.54
j95q03taq	15:10:19	329.13167	3.8	3.3	107.62	79.66
j95q03tbq	15:12:29	329.13318	3.6	3.2	107.60	79.63
j95q03tcq	15:14:39	329.13468	4.6	3.5	108.18	80.14
j95q03tdq	15:16:49	329.13619	3.8	3.4	107.78	79.88
j95q03teq	15:18:59	329.13769	3.6	3.5	107.85	79.91
j95q03tfq	15:21:09	329.13920	3.6	3.7	108.21	80.20

Rootname	Start (UT)	Time (HJD)	V2-rms	V3-rms	FWHM-x	FWHM-y
j95q03thq	15:23:19	329.14070	3.1	3.5	108.09	80.18
j95q03tiq	15:25:29	329.14221	3.2	3.5	108.80	80.93
j95q03tjq	15:27:39	329.14371	3.2	6.8	110.94	82.96
j95q03tkq	15:29:49	329.14522	3.3	6.5	111.80	83.69
j95q03tlq	15:31:59	329.14672	3.0	3.5	110.67	82.86
j95q03tmq	15:34:09	329.14823	3.3	6.1	111.95	83.90
j95q03v0q	16:24:35	329.18325	3.1	3.5	105.68	77.65
j95q03v1q	16:26:45	329.18475	3.5	3.8	105.95	77.93
j95q03v2q	16:28:55	329.18626	3.1	3.5	106.22	78.15
j95q03v3q	16:31:05	329.18776	3.0	3.4	106.26	78.26
j95q03v4q	16:33:15	329.18927	3.1	3.4	106.49	78.48
j95q03v5q	16:35:25	329.19077	3.8	3.3	106.77	78.69
j95q03v7q	16:37:35	329.19228	3.2	3.2	106.74	78.89
j95q03v8q	16:39:45	329.19378	7.8	7.0	107.94	79.95
j95q03v9q	16:41:55	329.19529	3.2	3.4	107.23	79.28
j95q03vaq	16:44:05	329.19679	2.9	3.3	107.29	79.27
j95q03vbq	16:46:15	329.19829	2.9	3.4	107.27	79.35
j95q03vcq	16:48:25	329.19980	3.1	3.5	107.34	79.49
j95q03vdq	16:50:35	329.20130	3.2	3.4	107.48	79.67
j95q03veq	16:52:45	329.20281	3.0	3.5	107.44	79.60
j95q03vfq	16:54:55	329.20431	3.1	3.3	107.37	79.64
j95q03vgq	16:57:05	329.20582	3.3	3.6	107.74	79.89
j95q03vhq	16:59:15	329.20732	3.6	3.5	108.00	80.12
j95q03viq	17:01:25	329.20883	3.2	3.3	108.41	80.65
j95q03vkq	17:03:35	329.21033	3.3	6.3	110.62	82.65
j95q03vlq	17:05:45	329.21184	3.0	3.4	109.87	82.17
j95q03vmq	17:07:55	329.21334	3.2	6.9	111.61	83.60
j95q03vnq	17:10:05	329.21485	3.2	7.8	112.09	84.05
j95q03voq	18:00:32	329.24988	3.7	3.5	105.59	77.67
j95q03vpq	18:02:42	329.25138	3.8	3.4	105.84	77.87
j95q03vqq	18:04:52	329.25289	4.3	3.4	105.95	78.02
j95q03vrq	18:07:02	329.25439	4.2	3.4	106.05	78.11
j95q03vsq	18:09:12	329.25590	3.8	3.3	106.29	78.37
j95q03vtq	18:11:22	329.25740	4.8	3.7	106.81	78.79
j95q03vuq	18:13:32	329.25891	4.9	3.7	106.79	78.89
j95q03vvq	18:15:42	329.26041	4.6	4.1	107.21	79.24

Rootname	Start (UT)	Time (HJD)	V2-rms	V3-rms	FWHM-x	FWHM-y
j95q03vwq	18:17:52	329.26192	4.8	3.6	107.33	79.36
j95q03vxq	18:20:02	329.26342	4.0	3.5	106.98	79.25
j95q03vyq	18:22:12	329.26493	4.1	3.5	107.22	79.39
j95q03vzq	18:24:22	329.26643	3.8	3.4	107.30	79.50
j95q03w0q	18:26:32	329.26794	4.6	4.0	107.80	79.89
j95q03w1q	18:28:42	329.26944	3.6	3.5	107.47	79.67
j95q03w2q	18:30:52	329.27094	3.9	3.5	107.42	79.61
j95q03w3q	18:33:02	329.27245	3.8	3.7	107.67	79.78
j95q03w4q	18:35:12	329.27395	3.3	3.4	107.72	79.83
j95q03w5q	18:37:22	329.27546	3.4	3.7	108.21	80.45
j95q03w6q	18:39:32	329.27696	3.0	3.4	109.01	81.36
j95q03w7q	18:41:42	329.27847	3.0	7.8	110.55	82.75
j95q03w8q	18:43:52	329.27997	2.8	3.4	109.65	81.98
j95q03w9q	18:46:02	329.28148	3.1	7.8	111.56	83.57
j95q03wuq	19:36:28	329.31650	3.0	3.1	104.99	77.29
j95q03wvq	19:38:38	329.31801	3.1	3.3	105.21	77.52
j95q03wwq	19:40:48	329.31951	2.7	3.3	105.48	77.67
j95q03wxq	19:42:58	329.32101	3.8	3.4	105.42	77.71
j95q03wyq	19:45:08	329.32252	3.7	3.3	105.78	78.03
j95q03wzq	19:47:18	329.32402	3.4	3.3	105.90	78.16
j95q03x0q	19:49:28	329.32553	2.8	3.1	105.93	78.22
j95q03x1q	19:51:38	329.32703	3.0	3.2	105.99	78.30
j95q03x2q	19:53:48	329.32854	2.6	3.1	105.98	78.33
j95q03x3q	19:55:58	329.33004	2.8	3.3	106.09	78.47
j95q03x4q	19:58:08	329.33155	2.6	3.1	106.17	78.57
j95q03x5q	20:00:18	329.33305	2.8	3.3	106.45	78.84
j95q03x6q	20:02:28	329.33456	2.5	3.2	106.37	78.71
j95q03x7q	20:04:38	329.33606	2.5	3.2	106.49	78.83
j95q03x8q	20:06:48	329.33757	2.7	3.3	106.47	78.87
j95q03x9q	20:08:58	329.33907	2.4	3.3	106.49	78.86
j95q03xaq	20:11:08	329.34057	2.6	3.5	106.69	79.04
j95q03xbq	20:13:18	329.34208	2.4	3.3	107.24	79.63
j95q03xcq	20:15:28	329.34358	2.5	3.4	107.99	80.46
j95q03xdq	20:17:38	329.34509	2.4	4.2	108.69	81.07
j95q03xeq	20:19:48	329.34659	2.5	8.0	110.78	82.82
j95q03xfq	20:21:58	329.34810	2.4	3.2	108.96	81.47